ORIGINAL PAPER

physica
p s s status
solidi

www.pss-a.com

Check for
updates

Light-Induced Degradation in Annealed and Electron Irradiated Silicon

Kevin Lauer,* Stefan Krischok, Thomas Klein, Mario Bähr, Alexander Lawerenz, Ralf Röder, Thomas Ortlepp, and Uwe Gohs

The composition of the defect, which is responsible for the boron–oxygen-related light-induced degradation (BO-LID) of the carrier lifetime in silicon, still remains an unresolved issue. It has been recently suggested that the BO-LID is due to the A_{Si}-Si_i-defect. Within this idea, the creation and discreation are governed by the interstitial silicon concentration. Annealing and electron beam (EB) irradiation are applied to influence the interstitial silicon concentration. The BO-LID is observed in the case of diffusion-oxygenated FZ (DOFZ) boron-doped silicon after annealing at 650 and 450 °C for 4 h, respectively. A nearly complete discreation of the BO-LID defect is found for the long-term high temperature (16 h at 1050 °C) anneal. This discreation process is explained by the diffusion of the interstitial silicon atoms to other sinks such as the wafer surfaces. The degradation of the carrier lifetime due to illumination after the EB irradiation is unambiguously related to the BO-LID phenomenon.

1. Introduction

Light-induced degradation (LID) of the carrier lifetime in silicon is a severe problem for the silicon-based devices like ultraviolet (UV) light detectors, solar cells, or radiation detectors. Due to its importance, LID has a long research history. A recent review article on LID was given by Lindroos and Savin.[1] It was found that an LID phenomenon appears in boron-doped and oxygen-contaminated silicon. Therefore, this phenomenon is often referred to as BO-LID.[2,3] Despite its long research history, the composition of the underlying defect center has not yet been identified.

Dr. K. Lauer, T. Klein, M. Bähr, Dr. A. Lawerenz, R. Röder, Prof. T. Ortlepp
CiS Forschungsinstitut für Mikrosensorik GmbH
Konrad-Zuse-Str. 14, 99099 Erfurt, Germany
E-mail: klauer@cismst.de

Dr. K. Lauer, Prof. S. Krischok
TU Ilmenau
Institut für Physik
Weimarer Str. 32, 98693 Ilmenau, Germany

Dr. U. Gohs[+]
Leibniz-Institut für Polymerforschung Dresden e. V.
Hohe Straße 6, 01069 Dresden, Germany

[+]Present address: Technische Universität Dresden, Institut für Leichtbau und Kunststofftechnik, Holbeinstr. 3, 01307, Dresden, Germany.

The ORCID identification number(s) for the author(s) of this article can be found under https://doi.org/10.1002/pssa.201900284.

There is some consensus that, in the case of boron-doped silicon, a boron atom on a substitutional site is involved in the defect center. The accompanying species was proposed to be an interstitial oxygen dimer.[4,5] Based on the degradation properties in B, Ga, and In-doped silicon, the authors suggested the involvement of an interstitial silicon atom, instead.[6,7] In the following, we will, despite the open discussion, denote this defect with BO-LID defect. There is a consensus on the origin of the observed defect kinetics. Responsible for the BO-LID defect kinetics tends to be an atomic reconfiguration rather than a long-range migration process.[5,8]

Herguth et al. found that a deactivation of the BO-LID defect is possible by a heat and illumination treatment.[9,10] The deactivation was proposed to be due to an attachment of hydrogen to the BO-LID defect.[11] We proposed a B_{Si}-Si_i-H_i-defect to be identical with the H3 center[7] measured in EB-irradiated silicon using the deep-level transient spectroscopy (DLTS) method.[12]

The creation of the BO-LID defect takes place during the crystal growth from an oxygen-contaminated melt and a subsequent cooling down of the crystal. It was noted that the position in the crystal has an impact on the BO-LID defect density.[13] Nevertheless, the creation process of the BO-LID defect is still to be found. In addition, it is also possible to discreate the BO-LID defect by thermal treatments. To investigate the creation and discreation process of the BO-LID defect, this article focuses on the impact of the thermal treatments and the EB irradiation on the BO-LID defect density. These thermal treatments and the EB irradiation are chosen as they impact the silicon interstitial density in silicon and thus can impact the BO-LID defect density.

2. Experimental Section

The wafers used for this experiment were made of <100> boron-doped p-type floating zone (FZ) and Czochralski (CZ) silicon with a diameter of 100 mm. The samples were divided into four groups. In **Table 1**, the resistivity ranges given by the wafer manufacturer, the wafer thickness, and the interstitial oxygen content[14] were summarized. CZ wafers had two groups, a group with a low and a group with a high doping density. They were denoted by CZ_l and CZ_h, respectively.

Table 1. Sample overview.

Groups	Resistivity [Ω cm]	Thickness [μm]	Interstitial oxygen concentration [cm^{-3}]
FZ	1–5	280	$<2 \times 10^{15}$
DOFZ	1–5	280	$(1.2 \pm 0.1) \times 10^{17}$
CZ_l	1–3	280	$(15.6 \pm 0.6) \times 10^{17}$
CZ_h	0.2–0.8	508	$(7.6 \pm 0.1) \times 10^{17}$

An oxygenation anneal was made for one FZ group. The diffusion-oxygenated FZ (DOFZ) group first received an oxidation anneal to grow 600 nm oxide. Then an annealing was made to in-diffuse the oxygen from the oxide layer into the FZ silicon wafer. This annealing was conducted at 1150 °C for 24 h under nitrogen atmosphere.

To investigate the BO-LID defect density, the carrier lifetime was measured using the microwave detected photo conductance decay (MWPCD) method.[21] The excess carrier density, at which the carrier lifetime was measured, was $\Delta n = 5 \times 10^{14}$ cm^{-3}. In the case of lifetimes below 1 μs and the CZ_h group, MWPCD transients were fitted by mono-exponential functions and the decay constant was interpreted as a carrier lifetime. In that case, the excess carrier density cannot be determined. However, we did not change the laser intensity and thus can assume that the carrier lifetime was measured in a similar excess carrier density range. Lifetime under illumination was measured automatically over at least one whole day. The illumination was done using the MWPCD excitation laser with an average intensity of $I_{av} = 8.5$ kWm^{-2}. The temperature of the sample during lifetime measurement and illumination was $T = 50$ °C. A BO-LID defect cycle consists of illumination for about one day with subsequent annealing for 10 min at 200 °C.

An example of lifetime measurements is given in **Figure 1**. At least two BO-LID defect cycles were investigated for each sample to ensure full reversibility. In Figure 1, the fast

recombination component (FRC) and the slow recombination component (SRC) of the BO-LID defect were clearly visible. To obtain the defect density of the SRC in groups FZ, DOFZ, and CZ_l, the inverse carrier lifetime τ_0^{-1} at $t_0 = 1000$ s is subtracted from the inverse carrier lifetime τ_1^{-1} at $t_1 = 80\,000$ s. In the case of group CZ_h, $t_0 = 100$ s was chosen. The FRC has not been analyzed in this investigation as some samples were iron contaminated and thus the lifetime in the FRC regime was affected by the acceptor iron pair (A_{Si}-Fe$_i$-) defect reactions. From averaging the defect density of several BO-LID defect cycles the reported error bars are decreased.

Five different annealing steps were applied to the wafers, which are summarized in **Table 2**. All annealing steps, except the 450 °C annealing step, were made under nitrogen atmosphere in a furnace. The furnace was at 600 °C when drive in and drive out of the wafers took place. Temperature ramps to the final processing temperature and back were 3.4 °C min^{-1}. All furnace-annealed wafers were RCA cleaned prior to annealing. In the case of the groups FZ, CZ_l and CZ_h the surfaces were blank silicon. In the case of the DOFZ group, the oxide layer was still present. These annealing steps were chosen as there were known changes in the oxygen configuration in silicon. Oxygen agglomerates and silicon interstitials were ejected as discussed in the discussion section.

To suppress the recombination of charge carriers at the surface of the wafers, a PECVD silicon nitride layer was deposited on both wafer surfaces.[22] The nitride layer was deposited after the furnace annealed and after removal of the oxide layer of the DOFZ group. Subsequently, the wafers were broken into 1×1 cm^2 small pieces.

Some pieces were annealed for 4 h at 450 °C. This annealing was made on a hot plate under room atmosphere. In addition, the 450 °C annealing was made after the silicon nitride layer deposition.

The EB irradiation was done at Leibniz-Institut für Polymerforschung Dresden e.V. using the electron accelerator ELV-2 (Budker Institute of Nuclear Physics, BINP, Russia).[23] The EB irradiation was performed in air atmosphere and at room temperature. Before EB irradiation, the samples were mounted on the conveyor system of the electron accelerator and passed under the electron exit window with a velocity of 12.2 mm s^{-1} to apply a dose of 80 kGy (2×10^{14} cm^{-2}) in steps of 2.5 kGy. The electron current was amounted to 0.2 mA. The electron energy was 1 MeV.
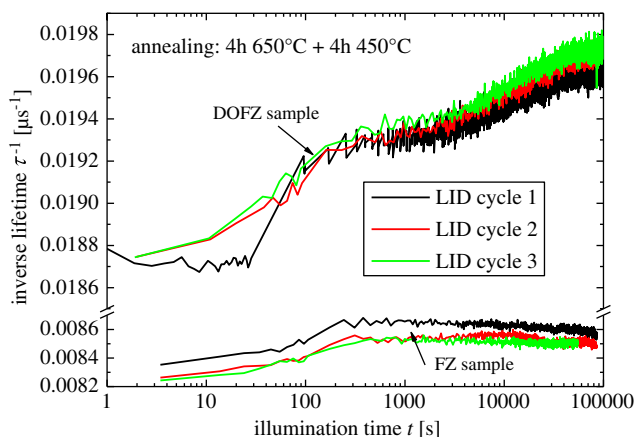

Figure 1. Inverse carrier lifetime as a function of illumination time is plotted for FZ and DOFZ samples, which underwent annealing steps for 4 h at 650 and at 450 °C. Three subsequent BO-LID defect cycles are shown. In case of the DOFZ sample, FRC and SRC are clearly visible.

Table 2. Annealing overview.

Annealing step	Description
4 h 450 °C	Formation of thermal double donors,[15] removal of radiation damage[16]
4 h 650 °C	Precipitation of silicon interstitials,[17,18] nucleation of oxygen precipitates[19]
4 h 750 °C	Nucleation of oxygen precipitates[20]
16 h 1050 °C	Precipitation of oxygen[20]
4 h 750 °C + 16 h 1050 °C	Nucleation of oxygen precipitates and precipitation of oxygen

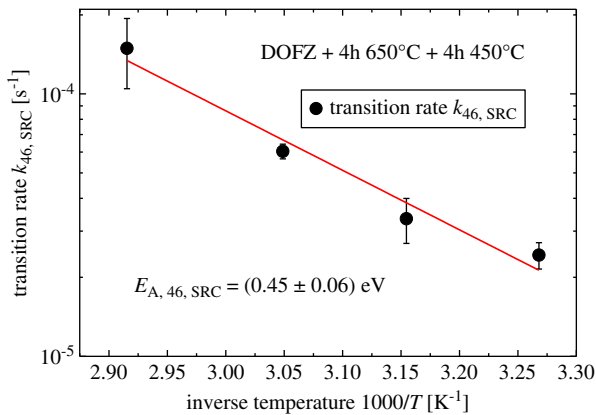**Figure 2.** The transition rate k46, SRC as a function of inverse temperature for the DOFZ sample from Figure 1. The activation energy E46, SRC is obtained from an Arrhenius fit of the data, indicated by a straight red line.

Figure 3. Inverse carrier lifetime as a function of illumination time for group CZ_h before and after annealing. For each sample three BO-LID defect cycles are plotted.

3. Results

3.1. Annealing

In Figure 1, the impact of the BO-LID on the carrier lifetime is clearly visible. In this diagram, the DOFZ group is shown after annealing for 4 h at 650 °C and 4 h at 450 °C, respectively. To verify that the observed degradation in the carrier lifetime is indeed the well-known BO-LID defect, we measured the activation energy of the SRC (see **Figure 2**). This was related to transition from state 4–6 of the current A_{Si}-Si_i-defect model.[8] A value of $E_{A, 46, SRC} = (0.45 \pm 0.06)$ eV is measured, which is in good agreement with data from the study[4] $E_{A, 46, SRC} = (0.475 \pm 0.035)$ eV.

In **Figure 3**, the inverse carrier lifetime during illumination is plotted for group CZ_h before and after annealing for 16 h at 1050 °C. The disappearance of the SRC due to the annealing step was clearly visible. In the highly doped group CZ_h, no FRC was visible.

Figure 4 shows the comparison of SRC defect densities for the four groups before and after stabilization anneal for 4 h at 450 °C. In the as-grown state, the FZ samples show an
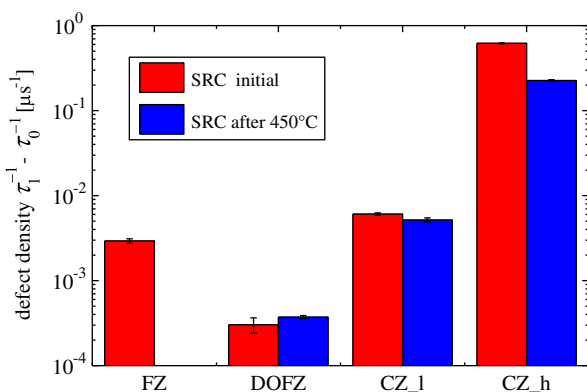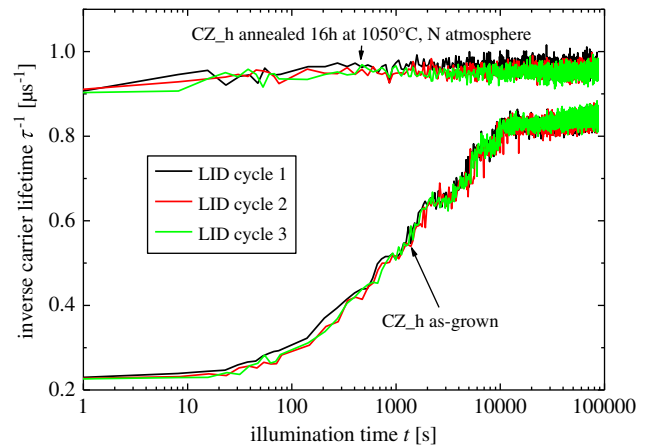
unexpected degradation due to illumination. This degradation can be removed by annealing for 4 h at 450 °C. However, the three other groups are only marginally influenced by this stabilization anneal. In the case of the CZ groups, the impact of boron doping on the defect density is clearly visible. Increasing the boron doping density increases the BO-LID defect density.

The impact of the annealing steps from Table 2 on the DOFZ, CZ_l, and CZ_h groups is depicted in **Figure 5–7**. It is noted that for each group and each furnace annealing step, the BO-LID defect density is decreased due to annealing. There is one exception. The 4 h at 650 °C annealing of the DOFZ group increases the BO-LID defect density. The observed decrease is most pronounced in each group for the long-term high temperature annealing step (16 h at 1050 °C).

A 4 h at 450 °C annealing step was made after the four furnace annealing steps and after the silicon nitride surface passivation deposition. In this case, an increase in the BO-LID defect density could be observed for both long-term annealing steps (see Figure 5–7).
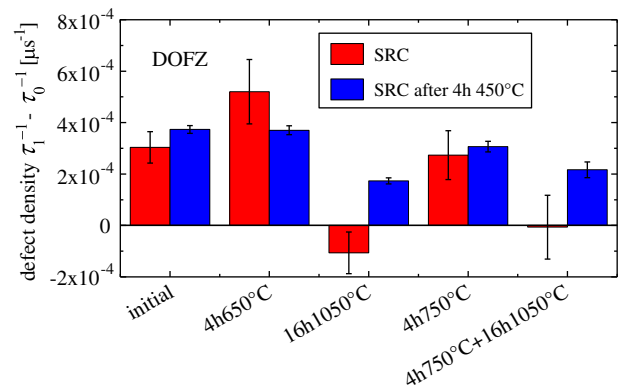

Figure 4. The defect densities of SRC measured in the four groups initially and after annealing for 4 h at 450 °C.

Figure 5. The defect densities of the SRC for the DOFZ group after different annealing steps. Blue columns indicate the SRC of the DOFZ group after an additional annealing for 4 h at 450 °C.
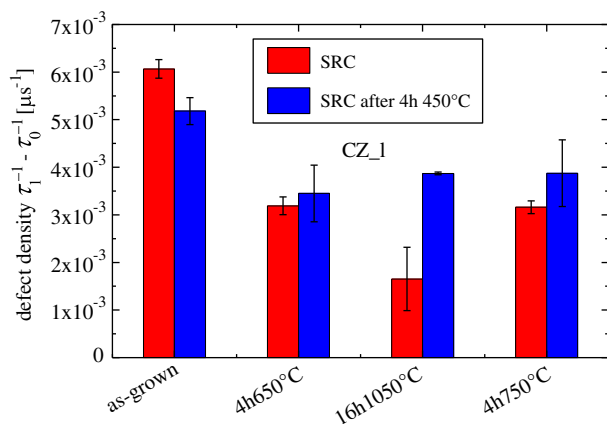
Figure 6. The defect densities of the SRC for the CZ_l group after different annealing steps and after an additional annealing step for 4 h at 450 °C.

Figure 7. The defect densities of the SRC for the CZ_h group after different annealing steps and after an additional annealing step for 4 h at 450 °C.

3.2. EB Irradiation

The results of the EB irradiation experiment are depicted in **Figure 8** and **9**. In Figure 8, the inverse carrier lifetime is plotted before and after EB irradiation for the four different groups. A strong increase in the inverse carrier lifetime is observed for the FZ, DOFZ, and CZ_l groups after EB irradiation. In Figure 9, three consecutive BO-LID cycles are shown for the FZ sample after EB irradiation. A weak reproducibility of the carrier lifetime changes after several BO-LID defect cycles is found.

4. Discussion

Within the A_{Si}-Si_i-defect model,[6–8,24,25] it is assumed that an acceptor atom with a silicon interstitial nearby is responsible for the BO-LID phenomenon in boron- and indium-doped silicon. The creation of this A_{Si}–Si_i-defect is due to a capture of a silicon interstitial atom by a substitutional acceptor atom and
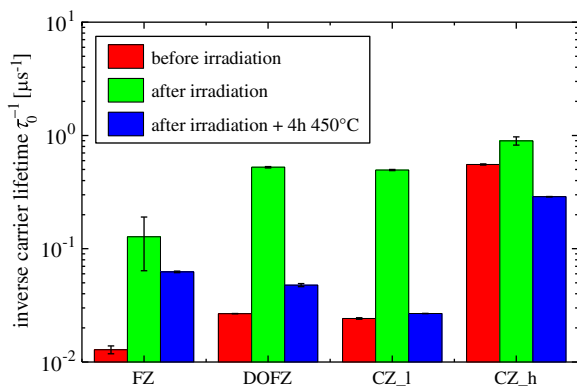
such captures take place during CZ crystal cooling.[7] The density of A_{Si}–Si_i-defects depends on several parameters: the acceptor concentration, the silicon interstitial concentration, the number of competing silicon interstitial sinks such as carbon or stacking faults present in the silicon, and the creation and discreation rate of the pairs.

The idea behind the annealing experiments applied in this investigation is to change the silicon interstitial concentration in the silicon. In consequence, the A_{Si}–Si_i-defect density should vary as well. From the understanding of the interplay of oxygen agglomeration, silicon interstitial generation, and silicon interstitial removal, one can draw conclusions on the BO-LID defect composition.

To draw a picture of what may happen during the applied annealing steps, we closely follow the current understanding of A_{Si}–Fe_i-defects. Interstitial iron is gettered by phosphorous-doped silicon during the high temperature phosphorous diffusion steps[26] or redistributed by iron precipitaton at low temperatures.[27] Similar reactions may take place in the case of silicon interstitials. Due to oxygen agglomeration, there is a continuous supply of silicon interstitials during the annealing

Figure 8. Inverse carrier lifetime measured in the four groups before and after irradiation with 1 MeV electrons of dose 2×10^{14} cm^{-3} and after an additional annealing step for 4 h at 450 °C. An increase of the inverse carrier lifetime and of the defect density due to irradiation is clearly visible.
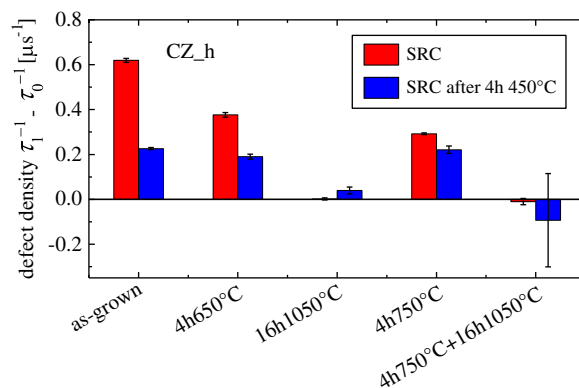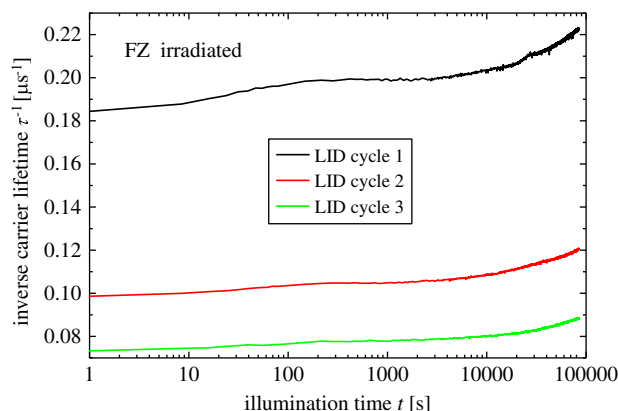

Figure 9. Inverse carrier lifetime as a function of illumination time for the FZ sample after irradiation. Three consecutive BO-LID defect cycles are shown.

steps.[28,29] It is assumed that the equilibrium between creation and discreation forms for the A_{Si}–Si_i-defects. The silicon interstitials are able to precipitate at 650 °C[18] in a similar way like interstitial iron precipitates at 500 °C.[27] This indicates that at 650 °C, the pressure for the silicon interstitial to form complexes, e.g. with an acceptor, due to super saturation seems to be high. In addition, the mobility of interstitial silicon is high enough to reach the sinks. From this, an increased equilibrium density of A_{Si}–Si_i-defects can be expected at 650 °C.

Probably, the equilibrium of the A_{Si}–Si_i-defect density will shift to the discreated or dissociated state with an increasing temperature. At an increased temperature, the freed silicon interstitial is able to move to other sinks. With a high A_{Si}–Si_i-defect density after crystal growth, this can explain the decrease in the A_{Si}–Si_i-defect density for high temperature annealing steps.

The FZ group shows an unexpected carrier lifetime degradation in the initial as-grown state (see Figure 4). This reversible degradation can be removed by a 4 h 450 °C anneal. The origin remains unclear, but it may belong to recently reported instabilities in as-grown FZ silicon.[30]

Five different annealing steps are applied to the four groups. The four furnace anneals lead with only one exception to a decrease in the SRC defect density (see Figure 5–7). The one exception is the 4 h anneal at 650 °C of the DOFZ group (see Figure 5). Herein, an increase in the SRC defect density is found. In this case, an interstitial super saturation, which is indicated by the formation of so-called {113} defects in this temperature region,[18] is present. The comparatively low defect density in the DOFZ group (see Figure 4) is the reason why an increase in the 650 °C anneal becomes visible.

The other groups and annealing steps lead to a decrease in SRC defect density. This may be explained by discreation or dissociation of the B_{Si}-Si_i-defect with subsequent redistribution of the silicon interstitial atoms to other sinks such as the surface, carbon, or stacking faults. Interestingly, the long-term high temperature anneal (16 h at 1050 °C) leads to a complete reduction of the SRC defect density for the groups DOFZ and CZ_h. At this temperature, the other sinks such as the surface or stacking faults are more attractive than the boron atom.

The 4 h at 450 °C anneal after the long-term high temperature anneal (16 h at 1050 °C), which strongly reduces the SRC defect density, leads to an increase in the SRC defect density in the DOFZ group (see Figure 5), whereas high SRC defect densities lead to a slight reduction in SRC defect density after the 450 °C anneal. This temperature region is known for the formation of the thermal donors. The underlying defects are still an open question.[19] However, oxygen agglomeration may also occur at this temperature with the consequence of emission of silicon atoms.[31,32] The decrease in SRC defect density for the CZ groups may also be explained by a redistribution of the interstitial silicon atoms after discreation or dissociation of the B_{Si}-Si_i-defect.

The results of the EB irradiation experiment are more difficult to explain. We found an increasing lifetime τ_0 with each BO-LID defect cycle (see Figure 9). In addition, the lifetime does not saturate under illumination. It was not possible to extract an activation energy from the measurements due to the mentioned problems. Therefore, we cannot be sure that the observed lifetime degradation under illumination is indeed caused by the BO-LID defect. The EB irradiation of silicon introduces vacancies as well. Thus, vacancy-related defects can also add recombination channels, which decrease the carrier lifetime.

Finally, we found that creation of the BO-LID defect takes place in oxygen-rich silicon at 650 °C. In addition, it is noted that discreation of the BO-LID defect is most pronounced due to long-term anneals at 1050 °C. Both findings can be explained within the frame of the A_{Si}–Si_i-defect theory. It cannot be ruled out that other explanation approaches exist. Thus, one has to state that the presented results do not allow to prove whether oxygen is involved in the BO-LID defect or not, but they open up a path to investigate the creation and discreation of the BO-LID defect further.

5. Conclusion

We have found the experimental conditions to create and to discreate the BO-LID. Starting from the idea of an A_{Si}–Si_i-defect model, it is assumed that a high silicon interstitial concentration is to be responsible for the creation of the BO-LID defect. Therefore, two ways were experimentally followed. First, we applied the annealing steps to agglomerate oxygen in the silicon matrix. This is accompanied by silicon interstitial generation. Second, EB irradiation of silicon was used to generate silicon interstitials as well as vacancies. By annealing DOFZ silicon for 4 h at 650 °C, we were able to create the BO-LID defect. In the case of the higher initial BO-LID defect densities, a decrease in defect density was observed after the annealing steps. This could be explained by a redistribution of the silicon interstitial atoms to other sinks such as the surfaces of the wafer, carbon, or stacking faults. The decrease in BO-LID defect density was most pronounced in the case of the long-term high temperature (16 h at 1050 °C) annealing step. For the low initial BO-LID defect density, the EB irradiation leads to an increase and for the high initial defect density, it leads to a decrease in the defect density. However, there remain doubts that in the case of EB irradiation the observed lifetime degradation under illumination is due to the BO-LID defect.

Conflict of Interest

The authors declare no conflict of interest.

[1] J. Lindroos, H. Savin, *Solar Energy Mater. Solar Cells* **2016**, *147*, 115.

[2] H. Fischer, W. Pschunder, in *Proceedings of the Tenth IEEE Photovoltaic Specialists Conf.*, IEEE, New York **1973**, p. 404.

[3] J. Schmidt, K. Bothe, *Phys. Rev. B* **2004**, *69*, 024107.

[4] K. Bothe, J. Schmidt, *J. Appl. Phys.* **2006**, *99*, 013701.

[5] V. Voronkov, R. Falser, *Phys. Status Solidi C* **2016**, *13*, 712.

[6] C. Möller, K. Lauer, *Phys. Status Solidi RRL* **2013**, *7*, 461.

[7] K. Lauer, C. Möller, D. Schulze, C. Ahrens, J. Vanhellemont, *Solid State Phenom.* **2015**, *242*, 90.

[8] K. Lauer, C. Möller, C. Tessmann, D. Schulze, N. V. Abrosimov, *Phys. Status Solidi C* **2017**, *14*, 1600033.

[9] A. Herguth, G. Schubert, M. Kaes, G. Hahn, *Prog. Photovoltaic Res. Appl.* **2008**, *16*, 135.

[10] A. Herguth, B. Hallam, *AIP Conf. Proc. 1999*, AIP Publishing, Melville, New York, USA **2018**, p. 130006.

[11] S. Wilking, A. Herguth, G. Hahn, *J. Appl. Phys.* **2013**, *113*, 194503.

[12] N. Yarykin, O. Feklisova, J. Weber, *Phys. Rev. B* **2004**, *69*, 045201.

[13] D. Walter, B. Lim, K. Bothe, R. Falser, V. Voronkov, J. Schmidt, in *27th European Photovoltaic Solar Energy Conf.*, WIP Munich, Frankfurt, Germany **2012**, p. 775.

[14] DIN EN 50513 (VDE0126-18):2009-12.

[15] P. Wagner, J. Hage, *Appl. Phys. A* **1989**, *49*, 123.

[16] I. Weinberg, C. K. Swartz, *Appl. Phys. Lett.* **1980**, *36*, 693.

[17] H. Bender, J. Vanhellemont, *Phys. Status Solidi A* **1988**, *107*, 455.

[18] D. Kot, T. Mchedlidze, G. Kissinger, W. von Ammon, *ECS J. Solid State Sci. Technol.* **2013**, *2*, P9.

[19] A. Borghesi, B. Piavac, A. Sassella, A. Stelle, *J. Appl. Phys.* **1995**, *77*, 4169.

[20] ASTM International, ASTM F 1239-94, https://webstore.ansi.org/standards/astm/astmf123994 (accessed: May 2019).

[21] K. Lauer, A. Laades, H. Übensee, H. Metzner, A. Lawerenz, *J. Appl. Phys.* **2008**, *104*, 104503.

[22] A. Laades, M. Blech, M. Bähr, K. Lauer, A. Lawerenz, *Phys. Status Solidi C* **2011**, *8*, 763.

[23] H. Dorschner, U. Lappan, K. Lunkwitz, *Nucl. Instr. Methods Phys. Res. B: Beam Interact. Mater. Atoms* **1998**, *139*, 495.

[24] C. Möller, K. Lauer, *Energy Procedia* **2014**, *55*, 559.

[25] K. Lauer, C. Möller, D. Schulze, C. Ahrens, *AIP Adv.* **2015**, *5*, 017101.

[26] S.M. Myers, M. Seibt, W. Schröter, *J. Appl. Phys.* **2000**, *88*, 3795.

[27] W.B. Henley, D.A. Ramappa, *J. Appl. Phys.* **1997**, *82*, 589.

[28] R. Jones, G. Watkins, *Early Stages of Oxygen Precipitation in Silicon*, Kluwer Academic Publishers, Dordrecht/Boston/London **1996**.

[29] U. Gösele, T. Y. Tan, *Appl. Phys. A* **1982**, *28*, 79.

[30] N. E. Grant, F. E. Rougieux, D. Macdonald, J. Bullock, Y. Wan, *J. Appl. Phys.* **2015**, *117*, 055711.

[31] W. Bergholz, J.L. Hutchison, P. Pirouz, *J. Appl. Phys.* **1985**, *58*, 3419.

[32] J. Vanhellemont, O. De Gryse, P. Clauws, *Phys. B: Condens. Matter* **2003**, *340–342*, 1056.